Neuron
Article

# Disynaptic Inhibition between Neocortical Pyramidal Cells Mediated by Martinotti Cells

Gilad Silberberg[1,2,*] and Henry Markram[1]
[1] Brain Mind Institute, Ecole Polytechnique Fédérale de Lausanne (EPFL), Lausanne CH-1015, Switzerland
[2] Nobel Institute for Neurophysiology, Department of Neuroscience, Karolinska Institute, Stockholm SE-17 177, Sweden
*Correspondence: gilad.silberberg@ki.se
DOI 10.1016/j.neuron.2007.02.012

## SUMMARY

**Reliable activation of inhibitory pathways is essential for maintaining the balance between excitation and inhibition during cortical activity. Little is known, however, about the activation of these pathways at the level of the local neocortical microcircuit. We report a disynaptic inhibitory pathway among neocortical pyramidal cells (PCs). Inhibitory responses were evoked in layer 5 PCs following stimulation of individual neighboring PCs with trains of action potentials. The probability for inhibition between PCs was more than twice that of direct excitation, and inhibitory responses increased as a function of rate and duration of presynaptic discharge. Simultaneous somatic and dendritic recordings indicated that inhibition originated from PC apical and tuft dendrites. Multineuron whole-cell recordings from PCs and interneurons combined with morphological reconstructions revealed the mediating interneurons as Martinotti cells. Martinotti cells received facilitating synapses from PCs and formed reliable inhibitory synapses onto dendrites of neighboring PCs. We describe this feedback pathway and propose it as a central mechanism for regulation of cortical activity.**

## INTRODUCTION

The neocortical microcircuit is characterized by a high degree of synaptic recurrence, in which excitatory, inhibitory, feed-forward, and feedback pathways are interweaved (Douglas and Martin, 1990; Markram et al., 2004; Miles, 1990; Szabadics et al., 2006; Thomson et al., 2002). Despite an overwhelming majority of excitatory synaptic connections, the balance between inhibition and excitation is dynamically maintained during cortical activity (Monier et al., 2003; Shu et al., 2003). Reliable activation of inhibitory pathways is essential for normal cortical activity, as excitation-inhibition imbalances are linked to various pathologies including epilepsy (Cobos et al., 2005; Cossart et al., 2001; Marco et al., 1996), schizophrenia (Lewis et al., 2005), anxiety (Powell et al., 2003), and hypersensitivity (Homanics et al., 1997). Neocortical interneurons mediating this inhibition are anatomically and electrically highly diverse (Karube et al., 2004; Markram et al., 2004) and are specialized to target different elements of postsynaptic neurons (Somogyi et al., 1998). Despite the vast knowledge regarding neocortical neurons and their synaptic connections, little is known about the multisynaptic pathways that maintain the crucial balance between excitation and inhibition.

The PCs in layer 5 constitute the main output layer of the neocortex, projecting to various subcortical brain areas including the striatum, brainstem nuclei, and spinal cord (Gao and Zheng, 2004; Killackey et al., 1989). The subpopulation of thick tufted PCs have dendrites that span across all cortical layers, enabling integration of activity from the entire width of the cortical sheet. The distal portions of their apical and tuft dendrites reside in layer 1, which is targeted by thalamic afferent input (Oda et al., 2004) and by top-down and multimodal afferents from other cortical areas (Cauller, 1995; Rockland and Pandya, 1979). Thick-tufted layer 5 PCs thus integrate local and distal inputs across all cortical layers and convey the integrated information downstream to the rest of the nervous system. It is therefore important to understand the pathways and mechanisms that regulate the activity of these neurons and prevent their overexcitation that would result in excess activation of their subcortical targets.

We describe here a prevalent disynaptic inhibitory feedback pathway between thick-tufted layer 5 neocortical PCs. This form of inhibition can be triggered by individual presynaptic neurons and displays unique spatial and temporal properties by affecting the dendrites of PCs in an activity-dependent manner. We characterize the electrophysiological, morphological and synaptic properties of this disynaptic inhibitory pathway and discuss its potential role in neocortical function.

## RESULTS

### Disynaptic Inhibition between Layer 5 PCs

We recorded from neighboring (lateral somatic distance less than 100 μm, mean, 46.6 μm) thick-tufted layer 5 PCs in slices of rat somatosensory cortex (see Experimental Procedures). When PCs were stimulated with trains of

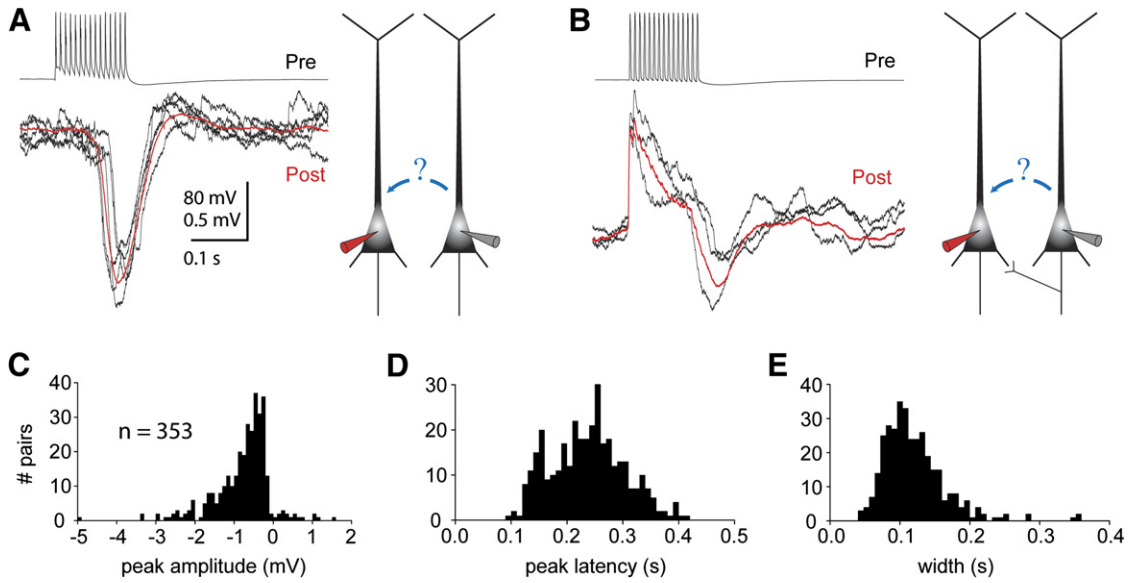


**Figure 1. Disynaptic Inhibition between Layer 5 PCs**

(A) Inhibitory responses evoked in the postsynaptic PC (post) by a 70 Hz train of 15 APs in a neighboring PC (pre). Examples of individual responses (black traces) are presented together with the average response of 30 repetitions (red trace).

(B) A biphasic excitatory-inhibitory response evoked in a PC following stimulation of a monosynaptically connected neighboring PC. Initial excitation due to a monosynaptic connection is followed by disynaptic inhibition. Trace coloring and scaling is as in (A).

(C) Histogram of the peak amplitudes of disynaptically connected PC pairs (n = 353 pairs). Peak amplitudes were extracted from average traces of at least 30 repetitions in which postsynaptic neurons were at resting membrane potential (−60.5 ± 5.3 mV).

(D) Histogram of the peak latency of disynaptic responses, as measured from the onset of the presynaptic AP train.

(E) Histogram of widths at half-amplitude of disynaptic responses.

action potentials (APs), we often observed inhibitory responses on neighboring PCs (Figure 1). Responses occurred only after presynaptic AP bursts and were not precisely time locked to the presynaptic AP trains. They were completely abolished following bath application of 10 μM NBQX (n = 10/10), indicating the participation of excitatory synaptic transmission. Unitary connections between layer 5 PCs are strongly depressing (Markram et al., 1997) and cannot evoke postsynaptic PC discharge under our experimental conditions, indicating that the observed inhibitory events were disynaptically mediated by intermediate interneurons. Inhibitory responses were observed between neurons that were not directly connected by an excitatory connection (Figure 1A) as well as in monosynaptically connected pairs (Figure 1B). The probability for such inhibitory disynaptic connections was more than double that of excitatory monosynaptic connections between PCs (disynaptic inhibition, 27%, 392 of 1450 examined pairs; monosynaptic excitation, 12%, 173 of 1450 pairs), suggesting high connection probabilities between PCs and the mediating interneurons. The fraction of disynaptically connected pairs that also had a monosynaptic excitatory connection between them was similar to the fraction of connected pairs in the entire population (13%, 52 of 392), indicating that disynaptic connections were formed without an apparent bias toward the existence of direct excitatory connections. We observed similar disynaptic inhibitory events in older (PN 25–30) animals as well (22%, 4 of 18 pairs), indicating that this pathway is not limited only to a narrow developmental period.

Apart from this delayed inhibition, we found in very few cases (4 of 1450 pairs, 0.3%) a different type of disynaptic inhibition, where inhibitory responses were evoked at the onset of the presynaptic train (Figure 2A). These disynaptic responses could be evoked by a single AP and did not require a presynaptic train of APs. This type of fast inhibition is mediated by interneurons receiving depressing excitatory synapses, in which the first EPSP response to an AP train is much larger than the following EPSPs (Galarreta and Hestrin, 1998; Silberberg et al., 2004; Figure 2B). In this study, we focused on the delayed disynaptic inhibition, which was abundantly triggered by single presynaptic PCs.

We used a presynaptic train of 15 APs at 70 Hz to characterize the inhibitory responses in 353 disynaptically connected PC (see Experimental Procedures). The peak amplitude of disynaptic responses was −0.8 ± 0.7 mV (values are all given in mean ± SD; range, −4.9 to +1.6 mV; Figure 1C), as measured in the soma at resting membrane potential (−60.5 ± 5.3 mV). The latency of the peak response relative to the onset of the presynaptic train was 241 ± 67 ms (94 to 410 ms; Figure 1D) and the width at half-amplitude of the response was 120 ± 46 ms (40 to 357 ms; Figure 1E).

The dependence of the disynaptic inhibition on presynaptic PC activity was examined by changing the frequency and the number of APs in the presynaptic train. The

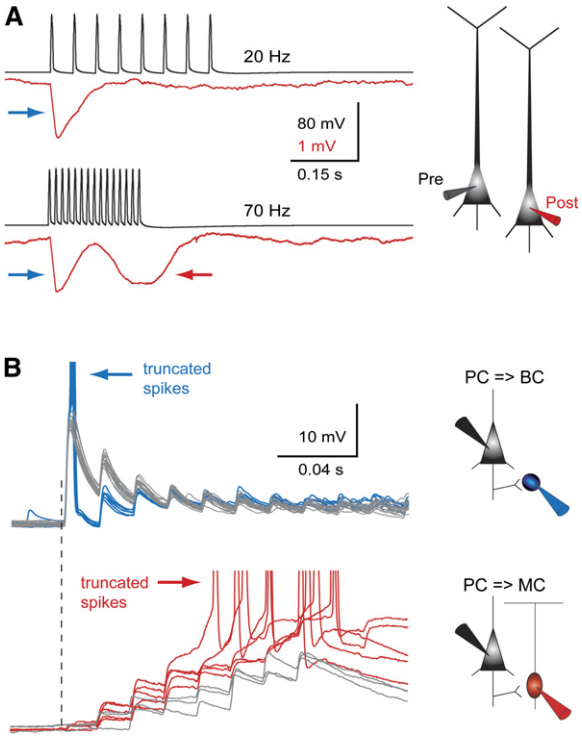


**Figure 2. Mechanisms Underlying Rate-Independent (Fast) and Rate-Dependent (Delayed) Disynaptic Pathways**

(A) Two PCs connected with both fast and delayed disynaptic connections. A 20 Hz presynaptic AP train evoked an immediate disynaptic response (upper traces), while a 70 Hz train induced both the immediate as well as a delayed rate-dependent response (lower traces). The immediate and delayed responses are designated by blue and red arrows, respectively. The frequency-independent component is mediated by a depressing PC to interneuron synapse (see blue trace in [B]). The delayed frequency-dependent component is mediated by a facilitating PC to interneuron synapse (see red trace in [B]).

(B) Monosynaptic connections between a layer 5 PC and a basket cell (upper traces), and between a layer 5 PC and MC (lower traces). The gray traces are those in which postsynaptic discharge was not evoked. Arrows show truncated APs and the dashed black line designates the presynaptic train onset.

magnitude and probability of disynaptic responses increased proportionally to the presynaptic frequency (Figures 2A and 3A). We systematically tested presynaptic frequencies between 30 and 70 Hz (trains of 15 APs) for characterization of this frequency dependence. The disynaptic response increased in amplitude and decreased in peak latency as a function of the frequency of the presynaptic AP train (n = 20/20; Figures 3A and 3B). Peak amplitudes of average disynaptic responses decreased by a 2-fold (to 51% ± 16%), and peak latencies increased (to 135.7% ± 9.6%) when presynaptic frequencies were changed from 70 to 50 Hz. The peak latency dependence on presynaptic frequency was fitted by an exponential function with a decay value of 17 Hz (Figure 3B). Disynaptic responses of this frequency-dependent type were rarely observed for frequencies lower than 20 Hz. We also examined the dependence of disynaptic responses on the duration of the presynaptic train by stimulating presynaptic PCs with different AP numbers with the same frequency (70 Hz). Disynaptic responses increased in amplitude and probability as more presynaptic APs were discharged (n = 24/24, Figures 3C and 3D). The relationship between the AP number and peak response amplitude was fitted by a single exponential function crossing the zero line at a value of 4.72 APs (Figure 3D), designating the average threshold for activating the disynaptic pathway under our conditions. In all trials, responses were never evoked by trains containing less than three APs. Our results demonstrate that this disynaptic pathway delivers inhibition that is tightly coupled to the level of PC activity.

## Disynaptic Inhibition Mediated by GABAa

Disynaptic responses were blocked in all cases when bicuculline (10 μM, n = 42), gabazine (10 μM, n = 12), picrotoxin (10 μM, n = 2) were applied to the bath solution, indicating that the observed inhibition was mediated by GABAa receptors (Figure 4A). In our experiments, the chloride concentration in the recording pipette was 10 mM, predicting a GABAa reversal potential of ∼−59 mV, after accounting for a junction potential of 9 mV. We verified this expected reversal potential for GABAa synaptic input by extracellular stimulation close to the PC soma in the presence of blockers for GABAb (100 μM CGP35348), NMDA (20 μM D-APV), and AMPA (10 μM CNQX) receptors and found it to be −57.5 ± 5.5 mV (n = 43). Most disynaptic responses (95%) were, however, hyperpolarzing at resting membrane potentials (−60.5 ± 5.3 mV) and even at more negative membrane potentials (Figure 1C). Conversely, when the pipette solution was replaced by a high-chloride solution (100 mM KCl, see Experimental Procedures), disynaptic responses were reversed and caused depolarization even at potentials close to −40 mV (n = 10), further indicating GABAa-mediated responses. In order to determine the effective somatic reversal potential of disynaptic inhibition under control conditions (10 mM KCl), we current-clamped the membrane at different holding potentials (Figure 4B). We then derived the effective somatic synaptic reversal potential by a linear fit to IPSP peak amplitudes as a function of the membrane holding potential (Figure 4C). The average effective reversal potential of the inhibitory responses (as recorded at the soma) was −78.9 ± 10.3 mV (n = 55), ranging between −112.9 and −58.2 mV (Figure 4D).

## Disynaptic Inhibition Targeted to Dendrites

The hyperpolarized somatic reversal potentials suggest that the disynaptic responses are mediated by inhibitory input targeted to dendrites of postsynaptic PCs. Distal dendrites are less affected by the somatic holding potential due to passive electrotonic attenuation (Spruston et al., 1993) and are more depolarized than the soma due to an exponential increase in the hyperpolarization activated inward current, Ih (Berger et al., 2001, Kole

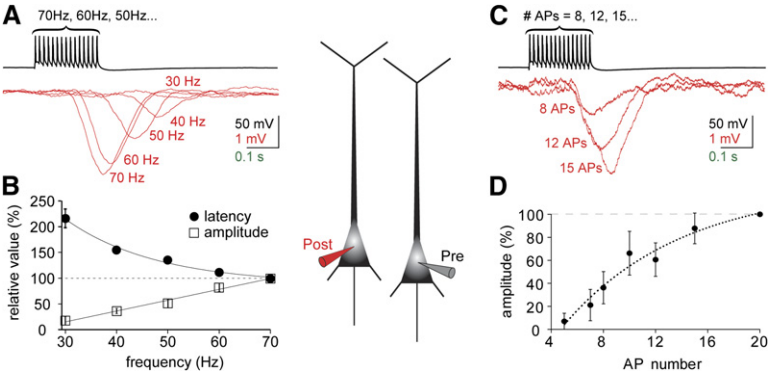


**Figure 3. Disynaptic Inhibition Depends on the Rate and Duration of Presynaptic Activity**

(A) Disynaptic inhibitory responses increased in amplitude and decreased in latency as a function of the presynaptic AP train frequency. Average responses (30 repetitions) to trains of 15 APs at frequencies of 30–70 Hz are shown (presynaptic example trace in black and postsynaptic traces in red).

(B) Peak latency (filled circles) and amplitude (open squares) are plotted as a function of the presynaptic AP train frequency (15 APs in all frequencies). The values for all cases (n = 20) are normalized to the response to a 70 Hz train (solid lines). Error bars represent the mean standard error of normalized values.

(C) Disynaptic responses increased in amplitude as a function of the number of APs in the train. Shown is an example of disynaptic inhibition between two PCs (presynaptic in black, postsynaptic in red). Presynaptic trains (70 Hz) with different AP numbers were evoked in the presynaptic PC (black), and average traces (30 repetitions) for each condition are overlaid.

(D) Disynaptic response amplitude is plotted as a function of the AP number (70 Hz trains). The values for all cases (n = 15) are normalized to the response to a 20 AP train. The data are fitted to a single exponent crossing the zero line at a value of 4.7 APs. Error bars represent the mean standard error of normalized values.

et al., 2006; Stuart et al., 1997). In addition, a somatodendritic gradient of chloride concentration is created by dendritic chloride pumps during whole-cell recordings (Khirug et al., 2005), causing a consequent gradient in GABAa reversal potential. These factors all contribute to the hyperpolarized reversal potential observed for the disynaptic inhibition. In order to test whether inhibition is exerted by synapses at distal portions of the PC dendrites, we performed simultaneous somatic and dendritic recordings from postsynaptic PCs while evoking AP trains in neighboring PCs (Figures 5A and 5B). Dendritic recordings were obtained from apical dendrites at distances between 250 and 550 μm from the soma (see Experimental Procedures). In all cases of simultaneous somatic and dendritic recordings of disynaptic inhibition (n = 10/10), the events recorded at the dendrites had faster rise times (measured between 10% and 90% of response amplitude) (Figure 5C), larger amplitudes (Figure 5D), and shorter peak latencies (Figure 5E) than at the soma. These differences were opposite for excitatory connections between PCs (Figures 5C and 5D), which mostly form synapses on basal dendrites (Kalisman et al., 2005; Markram et al., 1997). Figure 5B depicts an example where stimulation of the presynaptic neuron evoked a monosynaptic EPSP and

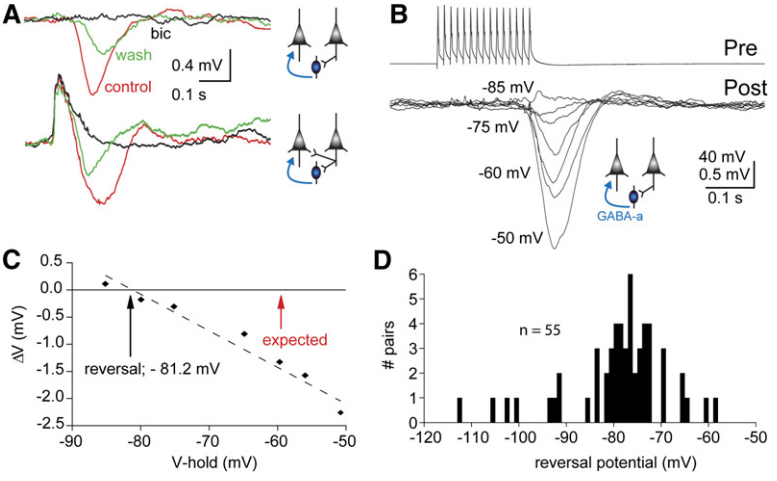


**Figure 4. Hyperpolarizing Somatic Reversal Potential**

(A) Disynaptic responses are blocked by bicuculine (10 μM), as shown in two examples. In the upper case, two PCs were connected disynaptically, and in the bottom case, two other PCs were connected disynaptically as well as monosynaptically, by an excitatory synapse. Average responses are shown for control conditions (red), in the presence of bicuculine (black), and 20 min after wash (green).

(B) The amplitude of disynaptic responses increased as a function of somatic membrane potential but was hyperpolarizing even when somatic voltage was held below −75 mV by negative current injection. Average traces of disynaptic responses are shown in black after baseline subtraction and holding potentials are written on the left.

(C) Extraction of reversal potential by linear fit of the example in (B). Amplitudes of disynaptic responses are plotted against the membrane holding potential, and the reversal potential is determined by the zero crossing of the linear fit (black arrow). The expected reversal potential for GABAa is marked by a red arrow. This value was calculated from the Nernst potential of chloride under experimental conditions, after correction for liquid junction potential of 9 mV. The expected reversal value was also confirmed experimentally by perisomatic extracellular stimulation in the presence of blockers for excitatory and GABAb synaptic transmission.

(D) Histogram showing reversal potential of 55 pairs, extracted in the same way as in (B) and (C). More than 95% of pairs had reversal values more hyperpolarized than expected for GABAa.

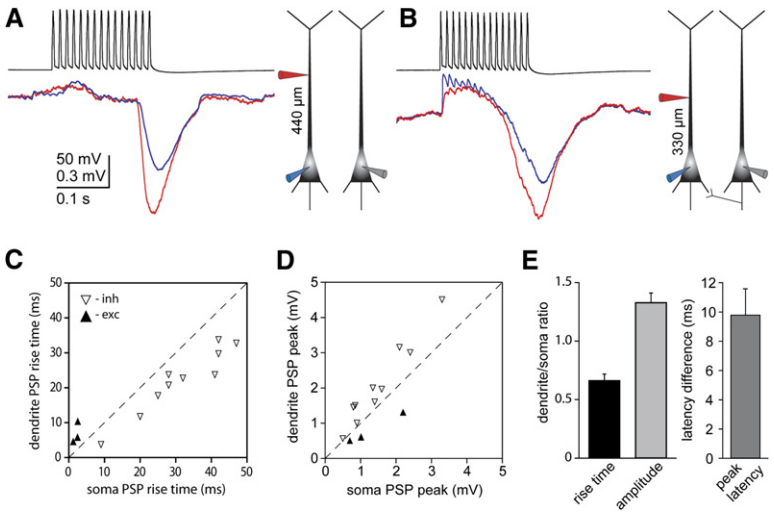


**Figure 5. Distal Disynaptic Inhibition Demonstrated by Combined Somatic and Dendritic Patch Recordings**

(A) A presynaptic PC was stimulated by trains of 15 APs at 70 Hz (black trace). Disynaptic events were recorded in the soma (average trace in blue) and apical dendrite (average trace in red) of a neighboring PC. Disynaptic events recorded at apical dendrites had larger amplitudes and shorter rise times than at the soma.

(B) A second example of presynaptic stimulation combined with postsynaptic somatic and dendritic recordings. In this case, the two PCs were connected monosynaptically as well as disynaptically. Monosynaptic EPSPs were larger and had shorter rise times in the somatic recording, whereas the inhibitory response was larger and faster in the dendritic recording. Excitatory connections between PCs are mainly formed on basal dendrites (Kalisman et al., 2005; Markram et al., 1997), which explains the attenuated excitatory response at the apical dendrite.

(C) The rise time (between 10% and 90% of peak amplitude) of disynaptic inhibitory responses (open triangles) as recorded at the soma (x axis) and dendrites (y axis) for 10 different connected pairs. Also plotted are the rise times of three cases of monosynaptic EPSPs (filled triangles). This suggests that excitatory synapses were located closer to the somatic recording pipette rather than the dendritic one, whereas the opposite occurs for disynaptic inhibitory inputs.

(D) The peak response amplitude (absolute value in relation to baseline) is plotted for somatic (x axis) and dendritic (y axis) recordings for the same PC pairs as in (C).

(E) The rise times, peak amplitudes, and peak delays of disynaptic inhibitory responses in somatic versus dendritic recordings. Ratios between dendritic and somatic rise times and peak amplitudes are shown in the left bar graph, and the differences in peak latencies are shown in the right bar graph. Error bars represent the standard error of the mean.

a disynaptic IPSP. While the EPSP is larger and faster in the soma, the following disynaptic inhibitory response is larger, faster, and earlier in the dendritic recording.

Apical and tuft dendrites of PCs express a high density of the hyperpolarization-activated inward current, Ih, with more than a 50-fold increase in channel density compared to the soma (Kole et al., 2006). This nonuniform distribution results in a depolarizing somatodendritic gradient of the resting membrane potential (Berger et al., 2001) as well as shortening of dendritic synaptic responses (Williams and Stuart, 2000). In order to assess the contribution of Ih in shaping the disynaptic responses, we applied the Ih blocker ZD7288 (50 µM) to the bath solution. Application of ZD7288 resulted in almost 3-fold widening of disynaptic responses (from 94 ± 11 to 258 ± 66 ms, n = 7) due to a pronounced prolongation of the decay time (see Figure S1 in the Supplemental Data available with this article online). Moreover, the overshoot following many of the disynaptic responses (examples in Figures 1, 4, 6, and S1) was abolished (Figure S1; n = 6/6), similar to previous reports for dendritic excitatory synapses (Berger et al., 2001; Williams and Stuart, 2000). Application of ZD7288 also resulted in an upwards shift of the effective reversal potential of disynaptic responses (n = 4/4; see Figure S1), toward the predicted GABAa reversal potential. These results show that the voltage gradient between PC soma and dendrites due to Ih (Berger et al., 2001) is one of the causes to the observed hyperpolarized reversal potential and further suggest the dendrites as the locus of inhibition.

## Martinotti Cells Mediate Disynaptic Inhibition

In order to study the origin of this disynaptic inhibition, we searched for the mediating interneuron by simultaneously recording from groups of close neighboring PCs and interneurons in layer 5 (cell bodies located less than 100 µm apart). We found complete disynaptic chains in 8 of 65 clusters, in which the presynaptic PC, intermediate interneuron, and the postsynaptic PC were all simultaneously recorded (examples in Figures 6 and 7C). In all morphologically identified clusters (n = 7/7), the intermediate neurons were Martinotti cells (MCs), as identified following biocytin staining (Figures 7 and S3). The defining morphological characteristic of this interneuron type is the axon collaterals that ascend to layer 1 (Braitenberg and Schüz, 1998; Fairen et al., 1984; Karube et al., 2004; Ramon y Cajal, 1891). Other morphological features of MCs are a beaded dendritic tree significantly smaller than the axonal tree, bitufted dendritic morphology, and an ovoid soma (also apparent under IR microscopy, see Figure 7A, left; Fairen et al., 1984; Karube et al., 2004; Kawaguchi et al., 2006; Wang et al., 2004). MCs displayed discharge accommodation in response to depolarizing step currents, a sag (overshooting) response to hyperpolarizing step currents (Figure 7B), and a low discharge threshold as previously reported (Goldberg et al., 2004; Karube et al., 2004; Kozloski et al., 2001; Wang et al., 2004).

Connections from PCs to MCs displayed pronounced facilitation and membrane summation, such that a presynaptic AP train in a single PC could evoke discharge

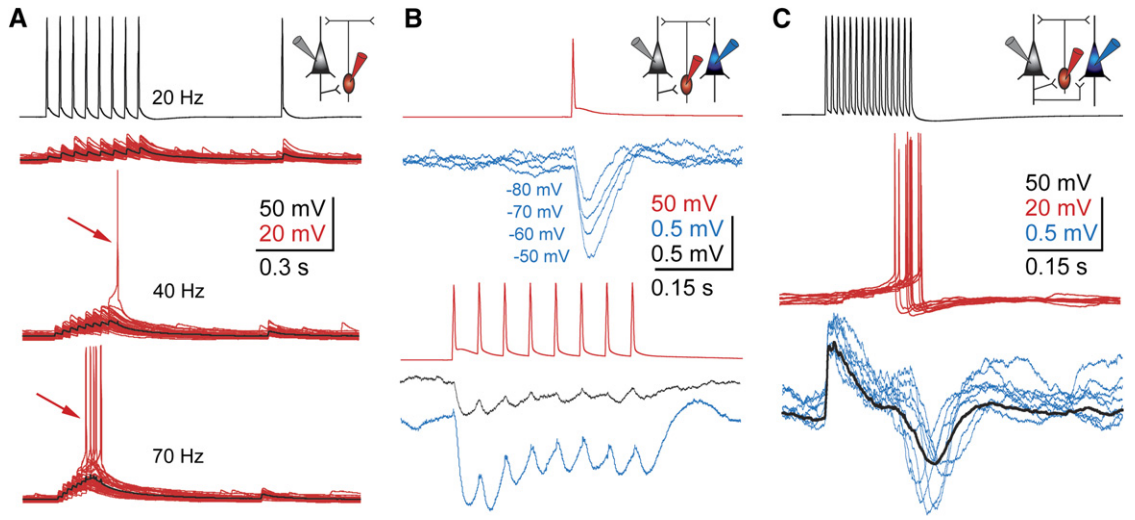


**Figure 6. Synaptic Properties of the Disynaptic Pathway**

(A) The PC to interneuron synapse. An example of an excitatory facilitating connection between a layer 5 PC (black traces) and MC (red traces). The presynaptic PC was stimulated with trains of eight APs at different frequencies (20, 40, and 70 Hz). Shown are examples of recordings from the postsynaptic MC (individual traces in red, average traces in black). Higher train frequency evoked postsynaptic APs with higher probability and shorter onset latency (indicated by red arrows), in agreement with the frequency dependence of disynaptic responses (Figures 3A and 3B).

(B) The interneuron to PC synapse. Depressing inhibitory connections between a layer 5 MC (red traces) and two neighboring PCs (blue and black traces). The PC in black was reciprocally connected to the MC and could evoke postsynaptic discharge following an AP train. The single IPSPs were recorded at different somatic holding potentials of the postsynaptic PC (upper traces), demonstrating the hyperpolarized synaptic reversal potential, similar to the values obtained for disynaptic responses (see Figure 4B). The same synaptic connection was activated by a train of eight APs at 20 Hz (lower traces), showing activity-dependent synaptic depression.

(C) The complete pathway. Example of a complete disynaptic connection, as recorded from two neighboring PCs and an intermediate MC. AP trains (70 Hz, 15 APs) evoked in the presynaptic PC (black) activated a facilitating connection in the postsynaptic MC (red traces). The synaptic activation was sufficient to evoke MC discharge, which resulted in IPSPs in the postsynaptic neighboring PC (blue traces, average of 30 sweeps in black).

in the postsynaptic MC (Figures 2, 6, and S2). Increasing presynaptic stimulation frequency caused a decrease in the latency of discharge onset and an increase of discharge probability (Figure 6A), in agreement with the results describing frequency dependence of the disynaptic responses (Figure 3A). Increasing the number of APs in presynaptic trains also increased the probability for postsynaptic discharge and in some cases induced discharge of several APs (see example in Figure S2). All connections from PCs to MCs (36/36) were facilitating, with low initial release probabilities (0.09 ± 0.12, 0.003 to 0.439), long facilitation time constants (670 ± 830 ms; range, 130 to 3212 ms), and short depression time constants (138 ± 211 ms; range, 6 to 418 ms), as derived from a model for synaptic dynamics (Markram et al., 1998) using average traces of at least 30 repetitions (see Experimental Procedures). Unitary EPSPs in these synapses were relatively small (0.28 ± 0.30 mV; range, 0.09 to 0.62 mV), but in response to presynaptic AP trains they facilitated (290% ± 360% amplitude increase between the first and second EPSPs) and summated on the postsynaptic membrane to a degree that could evoke postsynaptic MC discharge (n = 19 pairs; see example in Figure 2). The average latency to MC discharge from resting potential following 70 Hz AP trains in presynaptic PCs was 152 ± 42 ms (range, 60 to 240 ms; n = 21 pairs) corresponding to 10 APs on average, and never occurred before three presynaptic APs (minimal number of all trials in all pairs). Discharge onset displayed large trial-to-trial jitter (CV 20% ± 8%), indicating the lower temporal precision in the activation of the rate-dependent pathway, in comparison to the immediate response observed in the fast pathway (see Figure 2B for comparison).

The synaptic connections from MCs to PCs displayed synaptic depression (16/16 connections; Figure 6B), with higher release probabilities (0.30 ± 0.08; failure rate, 7.2% ± 9.4%; range, 0% to 30%), longer depression time constants (1250 ± 520 ms; range, 660 to 2480 ms), and very short facilitation (2 ± 4 ms; range, 1 to 14 ms). Monosynaptic IPSPs had small mean amplitudes (−0.5 ± 0.4 mV; range, −0.1 to −1.7 mV, recorded at a holding potential of −57.3 ± 3.2 mV), long rise times (16.1 ± 4.2 ms; range, 9.7 to 25.1 ms, measured between 10%–90% of the amplitude), and long peak latencies (27.4 ± 5.7 ms; range, 17 to 39 ms). These kinetics are longer than those we observed for synapses between basket cells and PCs (rise time, 6.3 ± 1.3 ms; peak latency, 15.9 ± 2.7 ms; n = 8), as expected for dendritic compared to perisomatic inhibition. The smaller amplitudes of monosynaptic IPSPs in comparison to the larger amplitudes of disynaptic events suggest the involvement of more than a single intermediate interneuron (see also Figure S2). Somatic

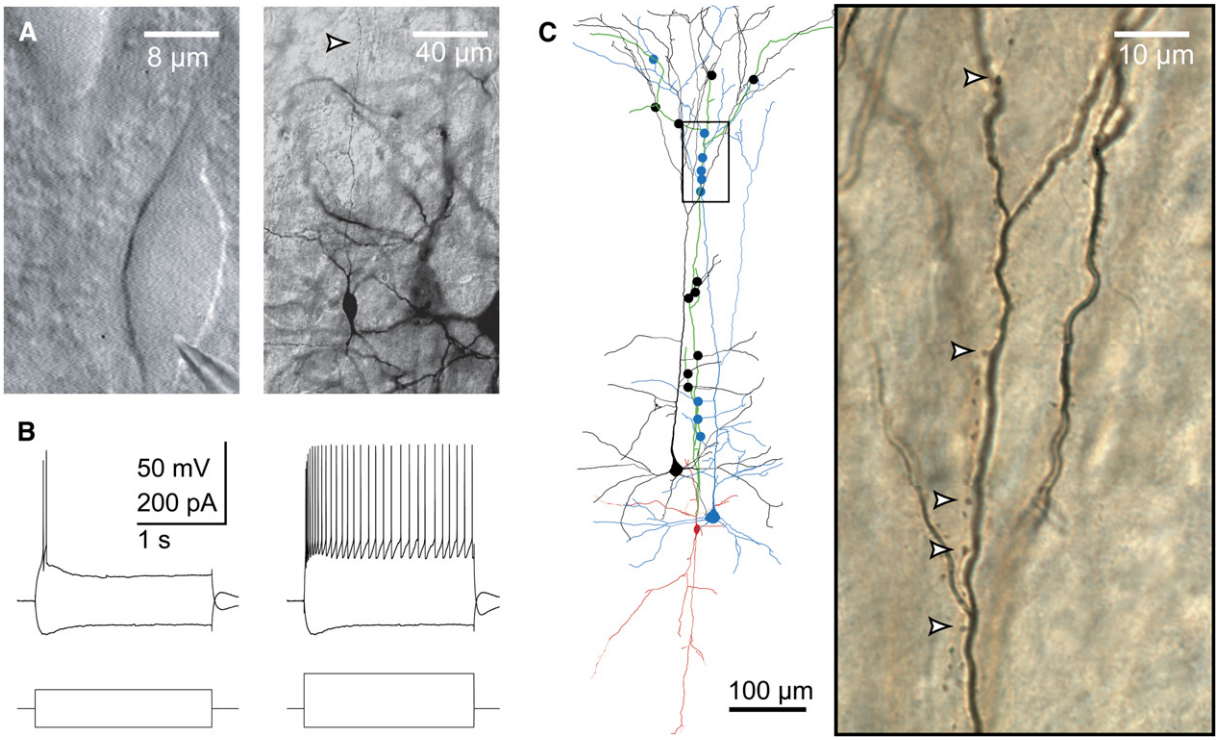


**Figure 7. Morphology and Electrophysiology of the Disynaptic Pathway**

(A) Typical bitufted morphology of a MC, as seen in IR-DIC microscopy during patch recordings (left), or under light microscopy after biocytin staining (right). The ascending axon is marked by a white arrowhead.

(B) Typical discharge pattern of a MC, displaying spike frequency accommodation and burst onset as a response to somatic step current injections.

(C) Morphological reconstruction of a MC and its synaptic contacts onto PCs (left). The MC (soma and dendrites in red, axons in green) contacted various locations of the dendrites of two neighboring PCs. Somata and dendrites of PCs are colored in black and blue. Putative synapses are labeled by filled circles with the same color as the target PC dendrites. The area marked by a black rectangle shows the enlarged image of five putative synaptic contacts (marked by white arrowheads), as obtained by light microscopy.

reversal potentials of these connections were more negative than the GABAa reversal potentials of monosynaptic connections (−88 ± 14 mV; range, −65.4 to −103.8; n = 6; see Figure 6B), similar to the values observed for disynaptic pairs (Figure 4D).

### A Spread of Postsynaptic Locations

We investigated the synaptic contacts from MCs to PCs by performing 3D morphological reconstructions of MC-PC connected pairs (see Experimental Procedures). Putative synaptic contacts were defined according to the existence of axo-dendritic appositions and an axonal bouton swelling (Figure 7C). Putative synapses were found in all reconstructed MC-PC pairs (12 ± 3 contacts per pair, n = 4 pairs), located on apical (25%), oblique (31%), and tuft (44%) dendrites of PCs (Figures 7C and S3). These data are consistent with previous classifications of MCs as dendritic targeting interneurons (Kawaguchi and Kubota, 1997; Somogyi et al., 1998). The distance between putative synaptic contacts and somata of PCs ranged between 186 and 1146 µm (593 ± 296 µm) along the dendrite (Figure S3). These values are significantly larger than distances reported for contacts between layer 5 PCs (Markram et al., 1997) and from basket cells to PCs (Gupta et al., 2000; Wang et al., 2002).

We calculated the electrotonic attenuation for 48 putative synaptic contacts using the 3D morphological reconstruction and computer simulations using the NEURON simulator (see Experimental Procedures and Figure S3). Voltage attenuation from the synaptic contact to the soma was calculated for steady state (DC) and for time-varying (AC) signals corresponding to PSPs at putative contacts (Figure S3). The DC attenuation (soma/dendrite voltage ratio) varied between 0.02 and 0.84 (0.30 ± 0.23, n = 48), and the AC signal attenuation was between 0.002 and 0.61 (0.11 ± 0.13). The attenuation for 21 synaptic contacts located on the dendritic tuft was 0.097 ± 0.076 and 0.014 ± 0.015 for DC and AC attenuation, respectively. The wide distribution of dendritic locations for the MC to PC putative synaptic contacts may account for the variability observed in amplitudes, latencies, and somatic reversal potentials of disynaptic responses, as all these values depend on the dendritic location of synaptic contacts.

Synaptic connections between PCs and MCs were also characterized by multiple putative contacts (8.6 ± 2.1 contacts per synaptic connection, n = 15 pairs). Synaptic

contacts were located at 134 ± 84 μm from MC somata (range between 22 and 337 μm), and targeted mainly dendritic branches between the third and fifth orders (ranging between first and sixth order, 4%, 11%, 21%, 32%, 18%, and 14%, respectively). Interestingly, synaptic contacts were unevenly distributed and mainly located at descending dendritic branches, below MC somata (104/126, 83% of synaptic contacts; see examples in Figure S3).

### High Recurrence of Disynaptic Connectivity

We observed a high degree of divergence, convergence, and reciprocity in disynaptic connections recorded from clusters of 3 or more neighboring PCs (examples in Figure S4). Divergence in connectivity was observed in 61% of connections (n = 183/300), convergence in 50% (n = 150/300), and 33% (n = 98/300) of disynaptic connections were reciprocal. This dense disynaptic connectivity suggests a high probability for monosynaptic interconnectivity between PCs and MCs. We observed such a high degree of monosynaptic connectivity in connected clusters of PCs and MCs, in which 68% of neighboring PCs contacted the same MC, and an even higher rate of MC to PC divergence, where MCs contacted 79% of neighboring recorded PCs. Convergence of PC to MC connectivity was also suggested from the cooperative stimulation of several presynaptic PCs, resulting in combined responses that were in many cases larger or smaller than the sum of individual responses (supra- and sublinear summation, respectively, see example for supralinear summation in Figure S4B). If the different presynaptic PCs would only engage nonoverlapping sets of interneurons, the responses would be expected to summate almost linearly, assuming only little dendritic nonlinear amplification of IPSPs. Supralinear summation could occur when individual activation of presynaptic PCs evokes interneuron discharge only with low reliability, but when two presynaptic PCs are coactivated, the target interneuron will discharge reliably. The observed nonlinear responses strongly indicate that interneurons were excited by several presynaptic neighboring PCs even in the reduced connectivity of the slice preparation. When recording from complete pathways (presynaptic PC, discharging intermediate MC, and a postsynaptic PC), we observed inhibitory responses also (1) when the intermediate MCs failed to discharge, (2) when the intermediate MCs were actively prevented from discharging by injection of hyperpolarizing current (Figure S2), (3) in other PCs that did not receive direct inhibition from the recorded MC. These inhibitory responses demonstrate the parallel activation of several interneurons in mediating the response and not only the single recorded MC. The amplitude of monosynaptic MC-PC connections was smaller than the disynaptic responses, ranging from 22% to 98% (65% ± 27%, n = 7). In four cases, we also quantified the contribution of the recorded interneuron to the overall response by comparing the response evoked by a single MC to the overall disynaptic response (Figure S2). In these experiments, we alternately prevented the recorded MC from discharge by injection of a hyperpolarizing current step at every second trial. We then subtracted the average postsynaptic response from the control response, in which the interneuron was allowed to discharge. The comparison yielded ratios of 1.1, 1.7, 2.2, and 2.5 between the amplitudes of the total disynaptic response and the response evoked by the single MCs, corresponding to 40%–90% contribution of a single MC to the overall response. The above data shows that the disynaptic interaction between PC pairs is mediated by several interneurons in parallel as a result of PC-MC divergence and MC-PC convergence. We recorded only from groups of neighboring layer 5 PCs and interneurons; thus, it is possible that part of the disynaptic response is mediated by more distal interneurons, perhaps in other layers. Our data predicts that these interneurons also receive facilitating synapses from PCs and provide GABAa mediated inhibition to PC dendrites.

In addition to the prevalent disynaptic connectivity between neighboring PCs, we also found a high prevalence of self-inhibition mediated by reciprocal PC-MC connections, with 77% of MCs in complete disynaptic clusters inhibiting also the presynaptic PCs (Figures 6B and 7C). In these cases, activation of the intermediate MC resulted in inhibition of the presynaptic PC as well as that of the neighboring PC. Disynaptic responses evoked in the presynaptic PC are not easily detected due to the large conductance accompanying the AP train, yet the reciprocal synaptic connections reveal the existence of such inhibitory feedback loops. Examples for MC inhibition of both the triggering (presynaptic) PC as well as a neighboring PC are shown in Figures 6 and 7 (electrophysiology and morphology, respectively). Our results show that MCs inhibit with high probability the same presynaptic PCs that initiate their activity, as well as closely neighboring PCs.

This high degree of convergence, divergence, and reciprocity in the connectivity between PCs and MCs results in a widespread inhibitory impact following burst activation of a single layer 5 PC. In addition to the monosynaptic excitation of a small fraction of neighboring PCs, high frequency activation exerts inhibition in a significantly larger number of PCs by recruitment of interneurons via facilitating synapses, suggesting that under different activity states, the impact of an individual PC on its neighbors can functionally transform from excitation to inhibition.

### Subcolumnar Feedback Inhibition

The prevalence of disynaptic events is striking in view of the small numbers of MCs in the neocortical microcircuitry (less than 5% of all cortical neurons [Markram et al., 2004; Wang et al., 2004]) and is due to the high degree of divergence and convergence in PC-MC interconnectivity (see previous section). The number of boutons on a layer 5 MC axon is roughly 3000, of which 90% are formed on PCs (Karube et al., 2004; Wang et al., 2004), yielding only a few hundreds of postsynaptic PCs targeted by a single MC. The dense connectivity between MCs and neighboring PCs together with the high degree of self-inhibition,

suggest that despite the wide arborization of the axons and dendrites of both MCs and PCs, MCs effectively inhibit PCs within subcolumnar dimensions. This preference of close neighboring PCs is due to the ascending axons of MCs forming multiple synaptic contacts on the apical and oblique dendrites as well as the distal tuft dendrites (Figures 7 and S3). More distal PCs, however, are likely to receive inhibition only to the tuft dendrites in layer 1, reducing both probability for synaptic connections and their visibility in somatic recordings. Indeed, disynaptic connectivity between PCs drops by almost a ten-fold for intersomatic distances larger than 50 μm (Rinaldi et al., 2005), indicating that this form of disynaptic inhibition may act mainly within the dimensions of neocortical minicolumns.

## DISCUSSION

We described a novel disynaptic inhibitory feedback pathway between neocortical PCs. In short, PCs in layer 5 of rat neocortex evoked inhibitory responses in neighboring PCs via a disynaptic pathway, following high-frequency trains of APs. The amplitude and latency of inhibitory responses depended on the presynaptic AP train duration and frequency. The prevalence of these inhibitory responses was more than twice that of direct excitatory connections between these neurons, as revealed by recordings of more than 1400 neuron pairs. Interneurons participating in this rate-dependent feedback inhibition were MCs, characterized by ascending axons and arborization in cortical layer 1. These interneurons receive facilitating excitatory connections from PCs and provide reliable, depressing, GABAergic input onto PC apical and tuft dendrites. As revealed by anatomy, electrophysiology, and pharmacology, stimulation of a PC induces delayed inhibition of the same presynaptic PC as well as its close neighbors. This pathway is therefore a feedback pathway, providing rate dependent self-inhibition for populations of neighboring thick-tufted layer 5 PCs. Interestingly, the axonal arborization of MCs exhibits substantial morphological overlap with the apical and tuft dendrites of thick-tufted PCs, ascending to layer 1 and spreading laterally therein. MCs are therefore not only involved in gain control of local PC populations, but provide a major source of inhibition to the tuft dendrites in layer 1, thus influencing dendritic integration.

Fragments of this pathway have been described in previous studies, including the activation of interneurons by train stimulation of single presynaptic PCs (Kozloski et al., 2001; Markram et al., 1998) and GABAergic inhibition of distal dendrites of PCs (Larkum et al., 1999; Perez-Garci et al., 2006). In the hippocampus, disynaptic inhibition was observed between neighboring PCs (Miles, 1990) and dendritic inhibition was shown to affect the generation of dendritic calcium spikes (Miles et al., 1996). Hippocampal interneurons inhibiting distal dendrites of PCs are the *oriens-lacunosum moleculare* cells. These interneurons share numerous features with neocortical MCs, in that they receive facilitating excitatory connections (Ali and Thomson, 1998), express somatostatin (Freund and Buzsaki, 1996), display discharge frequency accommodation and Ih-mediated sag response to hyperpolarizing current step (Ali and Thomson, 1998), and importantly, target the distal dendritic portions of PCs (Freund and Buzsaki, 1996). Dendritic inhibition of hippocampal PCs has also been shown to be activated by high-frequency stimulation of neighboring PC axons (Pouille and Scanziani, 2004), suggesting that this type of feedback inhibition is a common feature in cortical microcircuits. Disynaptic inhibition was, however, not observed within the subpopulation of nontufted layer 5 PCs projecting to the contralateral hemisphere (Le Be et al., 2007), pointing toward a specialization of this disynaptic pathway within the microcircuitry.

In our study, we focused on neighboring interneurons (within 100 μm somatic distance) and found only MCs as the interneurons participating in the described pathway. This does not rule out the possibility that other GABAergic neurons, perhaps neurons residing in other layers, that receive facilitating excitation (Kaiser et al., 2004; Reyes et al., 1998; Wang et al., 2002) and target PC dendrites are involved as well.

The described disynaptic pathway conveys the firing rate as well as the number of spikes discharged by the presynaptic PC, in accordance with models of excitatory facilitating synapses (Tsodyks et al., 1998). This type of disynaptic inhibition is therefore proportional to the activity level of neighboring PC populations. Another type of disynaptic inhibition is activated by the onset of presynaptic discharge, involving depressing excitatory synapses onto other types of interneurons (Figure 2). Activation of this immediate inhibitory pathway by individual presynaptic PCs was much less frequent under our experimental conditions but was facilitated by coincident discharge of several presynaptic PCs (Figure S4A). The two pathways convey different features of PC activity, suggesting that they have different functions during cortical activity.

The thick tufted PCs of layer 5 are the main source of cortical projections to the tectum, brainstem, and spinal cord, and this type of inhibition may ensure a controlled output even at high levels of excitation of the cortical column. The involvement in feedback self-inhibition rather than competitive processing suggests that this pathway is important in preventing overactivation of cortical PCs, which may be important in the prevention of epilepsy. Indeed, a correlation was described between selective loss of hippocampal somatostatin-positive dendritic-targeting interneurons and epileptic states (Buckmaster and Jongen-Relo, 1999; Cossart et al., 2001). Our results show that during low discharge rates, the main effect of PCs on neighboring PCs is excitatory via monosynaptic connections, but during high-frequency bursts, the impact switches and becomes predominantly inhibitory via the disynaptic pathway.

Besides its function as a mechanism to self-regulate neocortical activity, the disynaptic Martinotti pathway provides inhibition to distal PC dendrites in layer 1. In

neocortical PCs, inhibitory inputs to distal apical and tuft dendrites are largely attenuated by the passive cable properties, making them significantly less effective than perisomatic IPSPs in controlling somatic potential and discharge (Williams and Stuart, 2003). Input from individual GABAergic interneurons to the distal portions of apical dendrites of layer 5 PCs can, however, prevent the initiation of dendritic calcium spikes (Larkum et al., 1999). The Martinotti pathway therefore serves as a negative feedback capable of preventing the prolonged regeneration of calcium spikes. This is further supported by the fact that dendritic calcium spikes cause high-frequency bursting of PCs (Larkum et al., 2001; Oakley et al., 2001; Stuart et al., 1997). The high-frequency discharge of PCs is effective in causing MC discharge, which in turn inhibit the source of the calcium spike at the distal PC dendrites. Such inhibition of calcium spikes was demonstrated in hippocampal PCs by extracellular stimulation of dendritic-targeting inhibitory afferents (Miles et al., 1996). Distal apical and tuft dendrites of PCs are the targets of "top-down" cortical excitatory input. Inhibition of the distal PC dendrites therefore provides a cellular and synaptic mechanism to control the integration of long-range afferent input with local microcircuit processing.

To conclude, we reported here a prevalent inhibitory feedback pathway between neocortical pyramidal neurons and propose it as a key component in the neocortical microcircuit, affecting short- as well as long-range cortical processing.

## EXPERIMENTAL PROCEDURES

### Slice Preparation and Recordings

Parasaggital slices (300 μm thick) were obtained from Wistar rats (PN 14–16) according to the Swiss guidelines for animal experiments. Slices were cut in ice-cold extracellular solution then kept in 33°C–35°C for at least 30 min and then moved to room temperature (20°C–22°C) before recordings. Whole-cell patch recordings were performed at 35°C ± 0.5°C in layer 5 of the somatosensory cortex. Neurons were visualized using IR-DIC microscopy (Zeiss Axioskop). In order to preserve the entire span of dendritic and axonal trees of PCs and MCs, only parallel slices were used for experiments, as determined by the projection of PC apical dendrites. Recorded neurons were selected visually according to the somatic and dendritic morphology, and up to seven neighboring neurons with lateral somatic distances less than 100 μm (47 ± 35 μm) were simultaneously recorded (setup manufactured by Luigs & Neumann). PCs were easily distinguished from interneurons by their pronounced apical dendrite and large soma. MCs, however, were not identifiable as such under infrared microscopy and were classified only after electrophysiological recordings and biocytin staining. The extracellular solution (both for cutting and recording) contained 125 mM NaCl, 25 mM glucose, 25 mM $NaHCO_3$, 2.5 mM KCl, 2 mM $CaCl_2$, 1.25 mM $NaH_2PO_4$, 1 mM $MgCl_2$. Recordings were amplified using axopatch 200B amplifiers (Molecular Devices), filtered at 2 KHz, digitized (5–20 KHz) using ITC-18 (Instrutech), and acquired using PulseQ electrophysiology package (Funetics) running on Igor Pro (Wavemetrics). Patch pipettes with resistances of 5–10 MΩ and 15–20 MΩ were used for somatic and dendritic recordings, respectively, containing 110 mM K-gluconate, 10 mM KCl, 10 mM HEPES, 4 mM ATP, 0.3 mM GTP, 10 mM phosphocreatine, and 0.4%–0.5% biocytin. Access resistance was compensated throughout the experiments, and data were discarded when they increased beyond 30 MΩ or 60 MΩ for somatic and dendritic recordings, respectively. In most experiments, the chloride concentration in the recording pipette was 10 mM, predicting a GABAa reversal potential of ~−59 mV. In some experiments, KCl in the pipette solution was increased to 100 mM and K-gluconate was reduced to 20 mM in order to obtain a depolarized reversal potential for GABAa (~−5mV). Synaptic responses (both mono- and disynaptic) were stable and could be recorded up to several hours after obtaining whole-cell recordings without any apparent rundown. An intertrial interval of 15 s was used for disynaptic protocols to enable sufficient recovery of the inhibitory response.

### Electrophysiology

Disynaptic connections were quantified by stimulation of single presynaptic PCs with trains of 15 APs with a frequency of 70 Hz, with 15 s intervals between stimulation trials. APs were evoked by injection of 3 ms square pulses to presynaptic neurons. The existence of disynaptic responses was determined by a deviation of at least 2.5-fold from the baseline standard deviation in average traces of 30 trials. Average postsynaptic traces of at least 30 trials were used to characterize the disynaptic events by fitting them with a Gaussian function enabling extraction of the peak amplitude, latency, and width at half-amplitude of disynaptic responses. Experiments that determined the frequency and AP number dependence (as in Figure 3) were performed by shuffling stimulations of different frequencies and train durations, in order not to introduce a systematic bias. In experiments that determined the somatic reversal potential (Figure 5), holding currents were injected manually, and access resistance was checked and compensated before recording at each holding potential. Dendritic recordings were obtained from apical dendrites at distances between 250 and 550 μm, after following the ascending apical dendrite by using the IR-DIC optics. Transition from on-cell to whole-cell configuration was achieved in most cases by application of a short (2 ms) pulse of negative current injection and not by negative pressure as used in somatic recordings. This method provided higher stability of the pipette tip on the dendrite, resulting in lower access-resistance and less failures in obtaining whole-cell dendritic recordings. Parameters describing the dynamics of recorded synapses included the synaptic utilization parameter, U (equivalent to the average release probability), the time constants of recovery from depression (D), and facilitation (F). These parameters were extracted by using the model for synaptic dynamics as previously described (Markram et al., 1998; Tsodyks et al., 1998).

### Morphological Reconstruction and Analysis

Recorded neurons were filled with biocytin and stained for light-microscopy morphological identification and 3D reconstruction, according to the detailed procedure described previously (Wang et al., 2004). MCs were identified by their typical axonal arborization, ascending vertically up to layer 1, and bifurcating therein (Wang et al., 2004). Neurons were 3D morphologically reconstructed using Neurolucida (Microbrightfield) under light microscopy using an Olympus BX51 microscope fitted with a 60×/0.9 water-immersion objective (Olympus). Putative synaptic contacts were determined according to the existence of an axo-dendritic apposition and a presynaptic bouton swelling at the touch site (see Figure 7). Identification of synaptic contacts by light microscopy with biocytin staining has been used in previous studies of this kind and verified with electron microscopy (Lübke et al., 2000; Markram et al., 1997; Silver et al., 2003; Tamas et al., 1997, 1998, 2004; Wang et al., 2002). The reported correlation between light and electron microscopy is high (Markram et al., 1997; Silver et al., 2003; Wang et al., 2002), with light microscopy reported to typically underestimate contact numbers (Tamas et al., 1998, 2004). In order to extract the geometrical and electrotonic distances for the different synaptic location, we loaded the morphology file from Neurolucida into the NEURON simulator (Hines and Carnevale, 1997). Values for electrotonic attenuation and electrotonic distance, defined as the

natural logarithm of the voltage attenuation (Carnevale et al., 1995), were extracted for all synaptic contacts (Figure S3) using the path impedance tool in NEURON. The parameters used for simulations were as follows: Rm (specific membrane resistance) of 25,000 $\Omega cm^2$ and Ra (specific axial resistance) of 155 $\Omega cm$.

### Supplemental Data

The Supplemental Data for this article can be found online at http://www.neuron.org/cgi/content/full/53/5/735/DC1/.

## ACKNOWLEDGMENTS

We are grateful to T.K. Berger, A. El-Manira, S. Garcia, J.-V. Le Be, Y. Penn, M. Pignatelli, T. Rinaldi, and Y. Wang for help with experiments and comments on the manuscript. The study was supported by an EU grant to H.M and HFSP fellowship to G.S.

Received: August 14, 2006
Revised: December 4, 2006
Accepted: February 8, 2007
Published: February 28, 2007

## REFERENCES

Ali, A.B., and Thomson, A.M. (1998). Facilitating pyramid to horizontal oriens-alveus interneurone inputs: dual intracellular recordings in slices of rat hippocampus. J. Physiol. *507*, 185–199.

Berger, T., Larkum, M.E., and Luscher, H.R. (2001). High I(h) channel density in the distal apical dendrite of layer V pyramidal cells increases bidirectional attenuation of EPSPs. J. Neurophysiol. *85*, 855–868.

Braitenberg, V., and Schüz, A. (1998). Cortex: Statistics and Geometry of Neural Connectivity, Second Edition (Heidelberg, Germany: Springer-Verlag).

Buckmaster, P.S., and Jongen-Relo, A.L. (1999). Highly specific neuron loss preserves lateral inhibitory circuits in the dentate gyrus of kainate-induced epileptic rats. J. Neurosci. *19*, 9519–9529.

Carnevale, N.T., Tsai, K.Y., Claiborne, B.J., and Brown, T.H. (1995). The electrotonic transformation: a tool for relating neuronal form to function. In Advances in Neural Information Processing Systems, G. Tesauro, D.S. Touretzky, and T.K. Leen, eds. (Cambridge, MA: MIT Press), pp. 69–76.

Cauller, L. (1995). Layer I of primary sensory neocortex: where top-down converges upon bottom-up. Behav. Brain Res. *71*, 163–170.

Cobos, I., Calcagnotto, M.E., Vilaythong, A.J., Thwin, M.T., Noebels, J.L., Baraban, S.C., and Rubenstein, J.L. (2005). Mice lacking Dlx1 show subtype-specific loss of interneurons, reduced inhibition and epilepsy. Nat. Neurosci. *8*, 1059–1068.

Cossart, R., Dinocourt, C., Hirsch, J.C., Merchan-Perez, A., De Felipe, J., Ben-Ari, Y., Esclapez, M., and Bernard, C. (2001). Dendritic but not somatic GABAergic inhibition is decreased in experimental epilepsy. Nat. Neurosci. *4*, 52–62.

Douglas, R., and Martin, K.A.C. (1990). Neocortex. In The Synaptic Organization of the Brain, G.M. Shepperd, ed. (Oxford: Oxford University Press), pp. 389–438.

Fairen, A., DeFelipe, J., and Regidor, J. (1984). Nonpyramidal neurons; general account. In Cellular Components of the Cerebral Cortex, A. Peters and E.G. Jones, eds. (New York: Plenum Press).

Freund, T.F., and Buzsaki, G. (1996). Interneurons of the hippocampus. Hippocampus *6*, 347–470.

Galarreta, M., and Hestrin, S. (1998). Frequency-dependent synaptic depression and the balance of excitation and inhibition in the neocortex. Nat. Neurosci. *1*, 587–594.

Gao, W.J., and Zheng, Z.H. (2004). Target-specific differences in somatodendritic morphology of layer V pyramidal neurons in rat motor cortex. J. Comp. Neurol. *476*, 174–185.

Goldberg, J.H., Lacefield, C.O., and Yuste, R. (2004). Global dendritic calcium spikes in mouse layer 5 low threshold spiking interneurones: implications for control of pyramidal cell bursting. J. Physiol. *558*, 465–478.

Gupta, A., Wang, Y., and Markram, H. (2000). Organizing principles for a diversity of GABAergic interneurons and synapses in the neocortex. Science *287*, 273–278.

Hines, M.L., and Carnevale, N.T. (1997). The NEURON simulation environment. Neural Comput. *9*, 1179–1209.

Homanics, G.E., DeLorey, T.M., Firestone, L.L., Quinlan, J.J., Handforth, A., Harrison, N.L., Krasowski, M.D., Rick, C.E., Korpi, E.R., Makela, R., et al. (1997). Mice devoid of gamma-aminobutyrate type A receptor beta3 subunit have epilepsy, cleft palate, and hypersensitive behavior. Proc. Natl. Acad. Sci. USA *94*, 4143–4148.

Kaiser, K.M., Lübke, J., Zilberter, Y., and Sakmann, B. (2004). Postsynaptic calcium influx at single synaptic contacts between pyramidal neurons and bitufted interneurons in layer 2/3 of rat neocortex is enhanced by backpropagating action potentials. J. Neurosci. *24*, 1319–1329.

Kalisman, N., Silberberg, G., and Markram, H. (2005). The neocortical microcircuit as a tabula rasa. Proc. Natl. Acad. Sci. USA *102*, 880–885.

Karube, F., Kubota, Y., and Kawaguchi, Y. (2004). Axon branching and synaptic bouton phenotypes in GABAergic nonpyramidal cell subtypes. J. Neurosci. *24*, 2853–2865.

Kawaguchi, Y., and Kubota, Y. (1997). GABAergic cell subtypes and their synaptic connections in rat frontal cortex. Cereb. Cortex *7*, 476–486.

Kawaguchi, Y., Karube, F., and Kubota, Y. (2006). Dendritic branch typing and spine expression patterns in cortical nonpyramidal cells. Cereb. Cortex *16*, 696–711. Published online August 17, 2005. 10.1093/cercor/bhj015.

Khirug, S., Huttu, K., Ludwig, A., Smirnov, S., Voipio, J., Rivera, C., Kaila, K., and Khiroug, L. (2005). Distinct properties of functional KCC2 expression in immature mouse hippocampal neurons in culture and in acute slices. Eur. J. Neurosci. *21*, 899–904.

Killackey, H.P., Koralek, K.A., Chiaia, N.L., and Rhodes, R.W. (1989). Laminar and areal differences in the origin of the subcortical projection neurons of the rat somatosensory cortex. J. Comp. Neurol. *282*, 428–445.

Kole, M.H., Hallermann, S., and Stuart, G.J. (2006). Single Ih channels in pyramidal neuron dendrites: properties, distribution, and impact on action potential output. J. Neurosci. *26*, 1677–1687.

Kozloski, J., Hamzei-Sichani, F., and Yuste, R. (2001). Stereotyped position of local synaptic targets in neocortex. Science *293*, 868–872.

Larkum, M.E., Zhu, J.J., and Sakmann, B. (1999). A new cellular mechanism for coupling inputs arriving at different cortical layers. Nature *398*, 338–341.

Larkum, M.E., Zhu, J.J., and Sakmann, B. (2001). Dendritic mechanisms underlying the coupling of the dendritic with the axonal action potential initiation zone of adult rat layer 5 pyramidal neurons. J. Physiol. *533*, 447–466.

Le Be, J.V., Silberberg, G., Wang, Y., and Markram, H. (2007). Morphological, electrophysiological, and synaptic properties of corticocallosal pyramidal cells in the neonatal rat neocortex. Cereb. Cortex, in press. Published online November 23, 2006. 10.1093/cercor/bhl127.

Lewis, D.A., Hashimoto, T., and Volk, D.W. (2005). Cortical inhibitory neurons and schizophrenia. Nat. Rev. Neurosci. *6*, 312–324.

Lübke, J., Egger, V., Sakmann, B., and Feldmeyer, D. (2000). Columnar organization of dendrites and axons of single and synaptically coupled

excitatory spiny neurons in layer 4 of the rat barrel cortex. J. Neurosci. *20*, 5300–5311.

Marco, P., Sola, R.G., Pulido, P., Alijarde, M.T., Sanchez, A., Ramon y Cajal, S., and DeFelipe, J. (1996). Inhibitory neurons in the human epileptogenic temporal neocortex. An immunocytochemical study. Brain *119*, 1327–1347.

Markram, H., Lübke, J., Frotscher, M., Roth, A., and Sakmann, B. (1997). Physiology and anatomy of synaptic connections between thick tufted pyramidal neurones in the developing rat neocortex. J. Physiol. *500*, 409–440.

Markram, H., Wang, Y., and Tsodyks, M. (1998). Differential signaling via the same axon of neocortical pyramidal neurons. Proc. Natl. Acad. Sci. USA *95*, 5323–5328.

Markram, H., Toledo-Rodriguez, M., Wang, Y., Gupta, A., Silberberg, G., and Wu, C. (2004). Interneurons of the neocortical inhibitory system. Nat. Rev. Neurosci. *5*, 793–807.

Miles, R. (1990). Synaptic excitation of inhibitory cells by single CA3 hippocampal pyramidal cells of the guinea-pig in vitro. J. Physiol. *428*, 61–77.

Miles, R., Toth, K., Gulyas, A.I., Hajos, N., and Freund, T.F. (1996). Differences between somatic and dendritic inhibition in the hippocampus. Neuron *16*, 815–823.

Monier, C., Chavane, F., Baudot, P., Graham, L.J., and Fregnac, Y. (2003). Orientation and direction selectivity of synaptic inputs in visual cortical neurons: A diversity of combinations produces spike tuning. Neuron *37*, 663–680.

Oakley, J.C., Schwindt, P.C., and Crill, W.E. (2001). Dendritic calcium spikes in layer 5 pyramidal neurons amplify and limit transmission of ligand-gated dendritic current to soma. J. Neurophysiol. *86*, 514–527.

Oda, S., Kishi, K., Yang, J., Chen, S., Yokofujita, J., Igarashi, H., Tanihata, S., and Kuroda, M. (2004). Thalamocortical projection from the ventral posteromedial nucleus sends its collaterals to layer I of the primary somatosensory cortex in rat. Neurosci. Lett. *367*, 394–398.

Perez-Garci, E., Gassmann, M., Bettler, B., and Larkum, M.E. (2006). The GABAB1b isoform mediates long-lasting inhibition of dendritic $Ca^{2+}$ spikes in layer 5 somatosensory pyramidal neurons. Neuron *50*, 603–616.

Pouille, F., and Scanziani, M. (2004). Routing of spike series by dynamic circuits in the hippocampus. Nature *429*, 717–723.

Powell, E.M., Campbell, D.B., Stanwood, G.D., Davis, C., Noebels, J.L., and Levitt, P. (2003). Genetic disruption of cortical interneuron development causes region- and GABA cell type-specific deficits, epilepsy, and behavioral dysfunction. J. Neurosci. *23*, 622–631.

Ramon y Cajal, S. (1891). Sur la structure de l'ecorce cerebrale de quelques mammiferes. Cellule *7*, 3–54.

Reyes, A., Lujan, R., Rozov, A., Burnashev, N., Somogyi, P., and Sakmann, B. (1998). Target-cell-specific facilitation and depression in neocortical circuits. Nat. Neurosci. *1*, 279–285.

Rinaldi, T., Silberberg, G., and Markram, H. (2005). Autism as a disorder of hyperconnectivity of local microcircuits with enhanced learning and memory potential. Society for Neuroscience, Washington, DC.

Rockland, K.S., and Pandya, D.N. (1979). Laminar origins and terminations of cortical connections of the occipital lobe in the rhesus monkey. Brain Res. *179*, 3–20.

Shu, Y., Hasenstaub, A., and McCormick, D.A. (2003). Turning on and off recurrent balanced cortical activity. Nature *423*, 288–293.

Silberberg, G., Wu, C., and Markram, H. (2004). Synaptic dynamics control the timing of neuronal excitation in the activated neocortical microcircuit. J. Physiol. *556*, 19–27.

Silver, R.A., Lübke, J., Sakmann, B., and Feldmeyer, D. (2003). High-probability uniquantal transmission at excitatory synapses in barrel cortex. Science *302*, 1981–1984.

Somogyi, P., Tamas, G., Lujan, R., and Buhl, E.H. (1998). Salient features of synaptic organisation in the cerebral cortex. Brain Res. Brain Res. Rev. *26*, 113–135.

Spruston, N., Jaffe, D.B., Williams, S.H., and Johnston, D. (1993). Voltage- and space-clamp errors associated with the measurement of electrotonically remote synaptic events. J. Neurophysiol. *70*, 781–802.

Stuart, G., Schiller, J., and Sakmann, B. (1997). Action potential initiation and propagation in rat neocortical pyramidal neurons. J. Physiol. *505*, 617–632.

Szabadics, J., Varga, C., Molnar, G., Olah, S., Barzo, P., and Tamas, G. (2006). Excitatory effect of GABAergic axo-axonic cells in cortical microcircuits. Science *311*, 233–235.

Tamas, G., Buhl, E.H., and Somogyi, P. (1997). Fast IPSPs elicited via multiple synaptic release sites by different types of GABAergic neurone in the cat visual cortex. J. Physiol. *500*, 715–738.

Tamas, G., Somogyi, P., and Buhl, E.H. (1998). Differentially interconnected networks of GABAergic interneurons in the visual cortex of the cat. J. Neurosci. *18*, 4255–4270.

Tamas, G., Szabadics, J., Lorincz, A., and Somogyi, P. (2004). Input and frequency-specific entrainment of postsynaptic firing by IPSPs of perisomatic or dendritic origin. Eur. J. Neurosci. *20*, 2681–2690.

Thomson, A.M., West, D.C., Wang, Y., and Bannister, A.P. (2002). Synaptic connections and small circuits involving excitatory and inhibitory neurons in layers 2-5 of adult rat and cat neocortex: triple intracellular recordings and biocytin labelling in vitro. Cereb. Cortex *12*, 936–953.

Tsodyks, M., Pawelzik, K., and Markram, H. (1998). Neural networks with dynamic synapses. Neural Comput. *10*, 821–835.

Wang, Y., Gupta, A., Toledo-Rodriguez, M., Wu, C.Z., and Markram, H. (2002). Anatomical, physiological, molecular and circuit properties of nest basket cells in the developing somatosensory cortex. Cereb. Cortex *12*, 395–410.

Wang, Y., Toledo-Rodriguez, M., Gupta, A., Wu, C., Silberberg, G., Luo, J., and Markram, H. (2004). Anatomical, physiological and molecular properties of Martinotti cells in the somatosensory cortex of the juvenile rat. J. Physiol. *561*, 65–90.

Williams, S.R., and Stuart, G.J. (2000). Site independence of EPSP time course is mediated by dendritic I(h) in neocortical pyramidal neurons. J. Neurophysiol. *83*, 3177–3182.

Williams, S.R., and Stuart, G.J. (2003). Voltage- and site-dependent control of the somatic impact of dendritic IPSPs. J. Neurosci. *23*, 7358–7367.